JOURNAL OF GEOPHYSICAL RESEARCH, VOL. 85, NO. B8, PAGES 4337–4350, AUGUST 10, 1980

Mechanics of Discontinuous Faults

P. SEGALL[1] AND D. D. POLLARD

U.S. Geological Survey, Menlo Park, California 94025

Fault traces consist of numerous discrete segments, commonly arranged as echelon arrays. In some cases, discontinuities influence the distribution of slip and seismicity along faults. To analyze fault segments, we derive a two-dimensional solution for any number of nonintersecting cracks arbitrarily located in a homogeneous elastic material. The solution includes the elastic interaction between cracks. Crack surfaces are assumed to stick or slip according to a linear friction law. For an array of echelon cracks the ratio of maximum slip to array length significantly underestimates the difference between the driving stress and frictional resistance. The ratio of maximum slip to crack length slightly overestimates this difference. Stress distributions near right- and left-stepping echelon discontinuities differ in two important ways. For right lateral shear and left-stepping cracks, normal tractions on the overlapped crack ends increase and inhibit frictional sliding, whereas for right-stepping cracks, normal tractions decrease and facilitate sliding. The mean compressive stress between right-stepping cracks also decreases and promotes the formation of secondary fractures, which tend to link the cracks and allow slip to be transferred through the discontinuity. For left-stepping cracks the mean stress increases; secondary fracturing is more restricted and tends not to link the cracks. Earthquake swarms and aftershocks cluster near right steps along right lateral faults. Our results suggest that left steps store elastic strain energy and may be sites of large earthquakes. Opposite behavior results if the sense of shear is left lateral.

INTRODUCTION

Field studies have demonstrated that faults are discontinuous geologic features consisting of numerous discrete segments [*Brown,* 1970; *Vedder and Wallace,* 1970; *Sharp,* 1972; *Clark,* 1973]. Even in cross section, fault geometries are quite complex; individual segments have different lengths and orientations and may transect or truncate adjacent segments [*Bonilla,* 1979]. Commonly, fault segments form an echelon array with individual segments nearly parallel with the general trend of the fault. Echelon patterns are characterized as left stepping or right stepping by viewing the segments along trend and noting whether one must step to the left or right to reach the next segment. Discontinuous fault traces occur at all length scales, from fault segments ~100 km long on the Anatoli fault [*Allen,* 1968; *Dewey,* 1976] and those 1–20 km long on the San Andreas fault, through those tens of meters long in the San Rafael desert [*Aydin,* 1977], to those meters or centimeters long in mining-induced normal faults observed in South African gold mines [*Gay and Ortlepp,* 1979; *McGarr et al.,* 1979*a*]. Discontinuities are characteristic of dip slip as well as strike slip faults and are independent of length scale, rock properties, total fault slip, and tectonic setting. Discontinuities are, indeed, a fundamental feature of faults.

Both geologic and geophysical evidence indicates that discontinuities play an important role in the kinematics and dynamics of the faulting process. The distribution of slip following earthquakes often indicates that segments behave as discrete slipping surfaces. For example, following the 1968 Borrego Mountain [*Clark,* 1972, Figure 32] and 1966 Parkfield, California [*Lindh and Boore,* 1980, Figure 5], earthquakes, slip went to zero at the end of segments and was maximal near the middle of segments.

Observations of surface deformation, accumulated during many episodes of slip, associated with echelon offsets suggest a marked difference in behavior between left- and right-stepping offsets. For right lateral shear, left steps tend to produce local upwarps, while right steps produce 'pull apart' basins, or 'rhomb grabens.' An example of a left step on a right lateral fault is found along the northwest-striking Coyote Creek fault in southern California. The 1968 Borrego Mountain earthquake broke the surface along three segments of the Coyote Creek fault [*Clark,* 1972]. Between the ~10-km long northern and central segments, sedimentary strata are warped into an anticlinal dome, known as the Ocotillo Badlands [*Sharp and Clark,* 1972], with a topographic relief of ~200 m above the surrounding desert (Figure 1). An example of a right step on a right lateral fault occurs near the town of Brawley, California (Figure 2). The Imperial fault extends for ~60 km to the southeast into Baja California. From geophysical evidence, including seismic and geodetic data [*Johnson and Hadley,* 1976], the Brawley fault is inferred to extend ~30 km to the northwest. The right step between these faults is ~6 km. A topographic depression, with ~10 m of relief, known as Mesquite Lake is located within the right step. It is bounded on the east by the north-striking end of the Brawley Fault [*Sharp,* 1976] and on the southwest and northwest by the Imperial fault and by the north-striking terminal branches of the Imperial fault, respectively. Rhombic depressions similar to Mesquite Lake are quite common [*Clayton,* 1966; *Tchalenko and Ambraseys,* 1970]. *Rodgers* [1980] has investigated the development of such basins by considering the surface deformation near two offset dislocations.

Seismologic evidence indicates that surface fault geometries may extend to appreciable depths [*Aki,* 1978]. For example, the distribution of aftershocks from the Parkfield earthquake reflects the 1-km right-stepping echelon discontinuity of the surface fault trace [*Eaton et al.,* 1970]. The aftershock focal depths are between 3 km and 15 km. *Bakun et al.* [1980] point out the close correlation between the fault trace geometry and epicenter locations, rupture directivity, and aftershock clustering in their study of the 1973 Cienega Road earthquake. This correlation suggests that discontinuities of several hundred meters in the surface trace extend to depths of 5–8 km.

Mechanical analyses of faulting must include specification of the following: (1) the geometry of the region, (2) appropri-

[1] Also at the Department of Geology, Stanford University, Stanford, California 94305.

Paper number 80B0313.

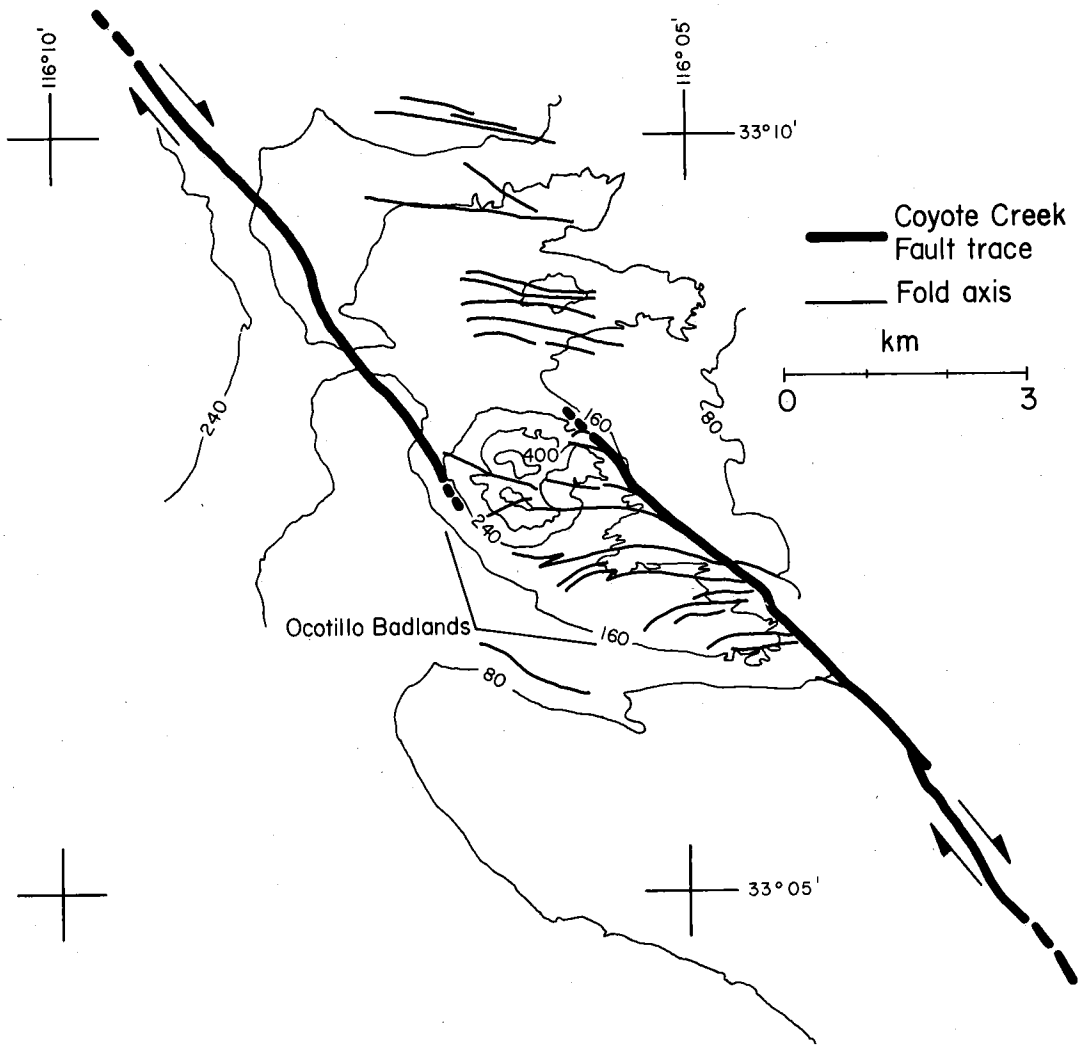

Fig. 1. Coyote Creek fault and Ocotillo Badlands in southern California. Contours indicate present elevation in feet, light lines represent traces of fold axes [after *Sharp and Clark,* 1972].

ate boundary and initial conditions, and (3) the constitutive behavior of all parts of the body. Considerable attention has been given to the constitutive behavior of the fault zone [*Rudnicki,* 1977; *Dieterich,* 1978; *Stuart,* 1979; *Stuart and Mavko,* 1979] and to boundary conditions specified as, for example, the level of tectonic stress or rate of plate motion [*Lachenbruch and Sass,* 1973; *Hanks,* 1977; *Zoback and Roller,* 1979]. Although geologists have described the geometry of faults in some detail [*Wallace,* 1973; *Bonilla,* 1979; *Wallace and Morris,* 1979], relatively little has been done to relate this geometry to the faulting process. Most workers have modeled the fault as a simple crack or dislocation [*Weertman,* 1965; *Chinnery,* 1968] or ellipsoidal inclusion [*Brady,* 1975; *Rudnicki,* 1977]. The principal objective of this paper is to present and discuss a model of a discontinuous fault composed of interacting segments. For tractibility, certain simplifying assumptions about the nature of the boundary conditions and the constitutive behavior are made.

The processes responsible for the formation of discontinuous faults are largely unknown and will not be considered here; rather, we investigate the consequences of preexisting discontinuities on stress and displacement fields in faulted regions. A general method for analyzing the elastic interaction of multiple cracks is outlined. The accuracy of the method is investigated by comparing computed results with those for a special case for which a closed-form solution is known. We then identify and explore two important effects of interaction for representative geometries. First, the importance of interaction in determining the distribution of tractions on cracks with frictional boundary conditions is examined. Next, the stress distribution in the region between cracks is studied. We also investigate the effect of multiple segments on the average stress change on the fault. These results are used to draw several general conclusions about the role of geometry in fault mechanics.

Method of Analysis

Each fault segment is analyzed as a discrete planar crack of fixed length and orientation in a homogeneous, linear elastic material. The far-field stress state is assumed to be spatially uniform, and the cracks are in static equilibrium. Because the stresses due to an individual crack, in an arbitrary array of cracks, decay with distance from the crack, the elastic interaction between cracks becomes less important at large separations. As a preliminary step, we estimate the range of crack separations for which the interaction is important.

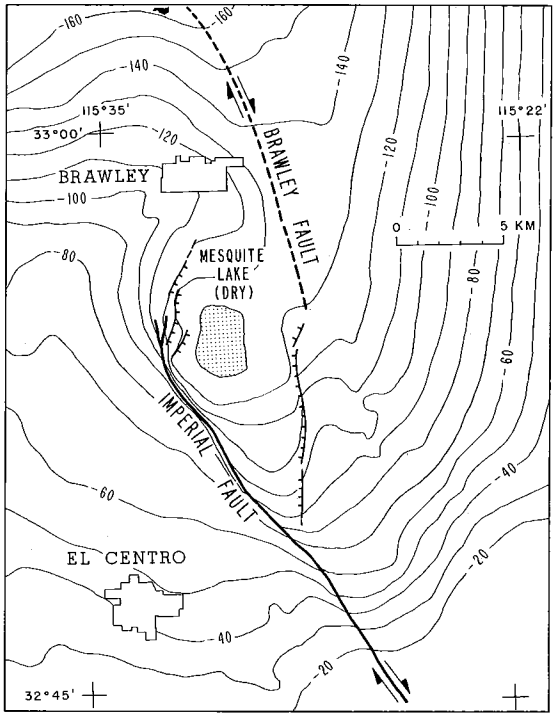

Fig. 2. Brawley and Imperial faults in Imperial Valley, California. Heavy lines denote major faults, dashed where inferred. The northern branches of the Imperial fault are illustrated as normal faults; in fact, the fault gradually changes character from strike-slip to oblique-slip to normal-slip. Topographic contours (light lines) delineate closed depression centered around Mesquite Lake [after *Johnson and Hadley*, 1976].

Strength of Crack Interaction

In two dimensions a crack is a line segment on which certain stress and displacement boundary conditions are satisfied. For an open crack, all tractions vanish on the line segment. The elastic fields are found by resolving the applied stresses acting on the line segment without the crack present σ_{ij}^a then adding the internal stresses that equal the negative of the applied stresses on the line segment and decay to zero at infinity. If the crack is isolated and the applied stresses σ_{ij}^a are uniform, the appropriate set of internal stresses is easily found [cf. *Paris and Sih*, 1965]. If, however, additional cracks are introduced, the elastic fields will be modified by interaction between cracks. In this case the resolved stress on the line segment becomes $\sigma_{ij}^a + \tilde{\sigma}_{ij}$, where $\tilde{\sigma}_{ij}$ are the nonuniform stresses contributed by all other cracks in the body. Interaction is important where the stresses due to other cracks make up a significant fraction of the total stress on a given crack, that is, when $\tilde{\sigma}_{ij}$ is some fraction ϵ of σ_{ij}^a.

A mode III crack can be thought of as a model of a strike slip fault of length that is much greater than depth a (Figure 3*a*). The stress distribution around a crack of half-length a parallel to the x axis and subjected to an antiplane stress σ_{yz}^a can be written as [*Paris and Sih*, 1965]

$$\sigma_{yz} + i\sigma_{xz} = \sigma_{yz}^a [1 - (a/\xi)^2]^{-1/2} \tag{1}$$

where $\xi = x + iy = r \exp(i\theta)$, r is the radial distance from the crack center, and θ is the angle measured counterclockwise from the crack plane. For $(a/\xi) < 1$, i.e., for distances greater than the half length, (1) can be expanded in a binomial series:

$$\sigma_{yz} + i\sigma_{xz} = \sigma_{yz}^a[1 + \tfrac{1}{2}(a/\xi)^2 + \tfrac{3}{8}(a/\xi)^4 + \cdots] \tag{2}$$

The perturbing stress is equal to the total stress minus the applied stress, where the applied stress is the first term in brackets in (2). Retaining terms of order $(a/\xi)^2$, the perturbing stress is given by

$$\tilde{\sigma}_{yz} + i\tilde{\sigma}_{xz} = \tfrac{1}{2}\sigma_{yz}^a(a/r)^2 \exp(-2i\theta) \tag{3}$$

These perturbing stresses are less than the prescribed fraction of the applied stress, that is, $\tilde{\sigma}_{ij} \leq \epsilon\sigma_{ij}^a$, outside a critical radius r_c. Noting that the θ-dependent term does not exceed unity, we find

$$r_c \cong a(2\epsilon)^{-1/2} \tag{4}$$

Choosing $\epsilon = 0.1$, we find $r_c = 2.25a$. Beyond this radius the perturbing stress is less than 10% of the applied stress.

We would expect significant interaction between faults if they are separated by less than twice the depth of faulting. For strike slip faults in California, seismicity is observed to depths of 10–15 km. Taking this to represent the depth of slip a, in-

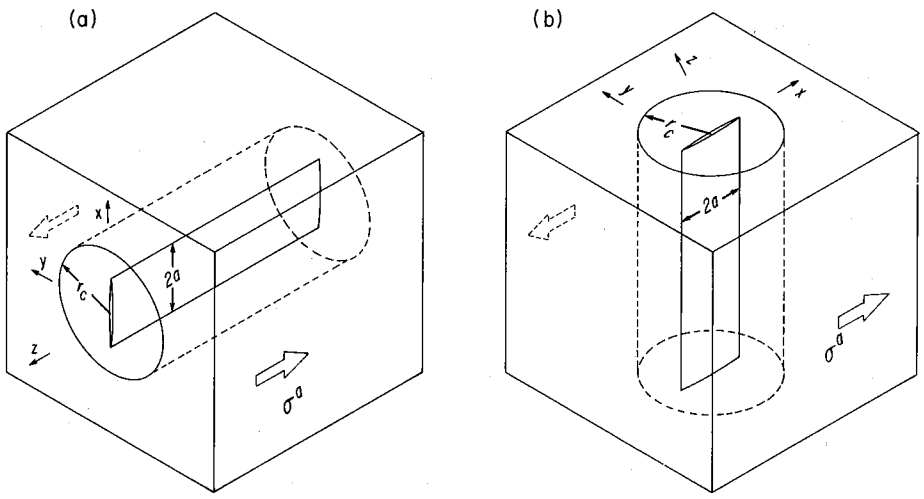

Fig. 3. Geometry for determination of interaction length scale: (*a*) antiplane (mode III crack) case; (*b*) plane strain (mode II crack) case; a is the crack half length; r_c defines a circular cylindrical region within which elastic interaction is significant.

teraction will be important if the faults are separated by less than 20–30 km. If the fault length is much less than the depth, an appropriate model is the plane strain (mode II) crack (Figure 3*b*). The stress distribution about a plane strain crack can also be expanded in even powers of (a/ξ). The critical radius for this case (with $\epsilon = 0.1$) is between $2a$ and $3a$. For strike slip faults in California, segments are typically separated by one tenth of their lengths. Therefore the interaction between segments and between adjacent faults is significant in many localities and should be included in analyses of the deformation and stress near faults.

Analysis of Interacting Cracks

Figure 4 illustrates the class of problems treated here. An infinite, homogeneous, isotropic, elastic material with shear modulus μ and Poisson's ratio ν is subject to uniform stresses at infinity. The far-field principal stresses σ_1^∞ and σ_3^∞ are oriented at an angle β with respect to a global coordinate system (X, Y). Any finite number of nonintersecting planar cracks may be introduced; each crack is defined by the coordinates of its center (X_i, Y_i), its half-length a_i, and the angle α_i that the crack plane makes with the X axis. A local coordinate (x_i, y_i) associated with each crack is oriented with x_i parallel to the crack plane. The problem considered here is two dimensional (plane stress or plane strain); that is, variations in stresses and fault geometry in the Z direction are negligible.

Solutions to multiple-crack problems have been found for several special geometries, such as infinite, periodic arrays of cracks [*Koiter,* 1961; *Delameter et al.,* 1975]. The general problem of arbitrarily located and oriented opening mode cracks was investigated by *Pucik* [1972] and *Ishida* [1973]. *Yokobori et al.* [1971] consider the problem of two echelon cracks in tension. The technique employed in this report is known as the Schwarz-Neumann alternating technique or the method of successive approximations [*Muskhelishvili,* 1954; *Sokolnikoff,* 1956]. Because the stresses everywhere are uniquely defined by the boundary tractions, we need only to guarantee that the boundary conditions are met on all internal surfaces (cracks) to find the complete stress and displacement distributions. The Schwarz-Neumann method involves first approximating the desired boundary conditions on a single crack, thus altering the stresses everywhere in the material, specifically on all other cracks. Next, the stresses on a second crack are adjusted to meet the desired boundary conditions, thus further altering the stresses on all other cracks. The boundary conditions are successively corrected, on each crack in turn, until they are satisfied within a given tolerance on all cracks.

It is worth emphasizing the differences between solutions which include the elastic interaction and those which simply superimpose the elastic fields of noninteracting cracks [*Kranz,* 1979] or dislocations [*Rodgers,* 1980]. In these solutions, all segments act independently; that is, during slip on one segment, all other segments are viewed as bonded together. The deformations from each segment acting alone are added together, a technique equivalent to the zeroth-order interaction in the Schwarz-Neumann method. The method presented here considers the complete interaction for slip on all segments affected by every other segment. The interaction is important to consider, especially when slip on adjacent segments, or faults, is known to occur simultaneously as creep events or earthquakes.

To approximate an arbitrary, nonuniform stress distribution on a single crack, we employ the fundamental solution,

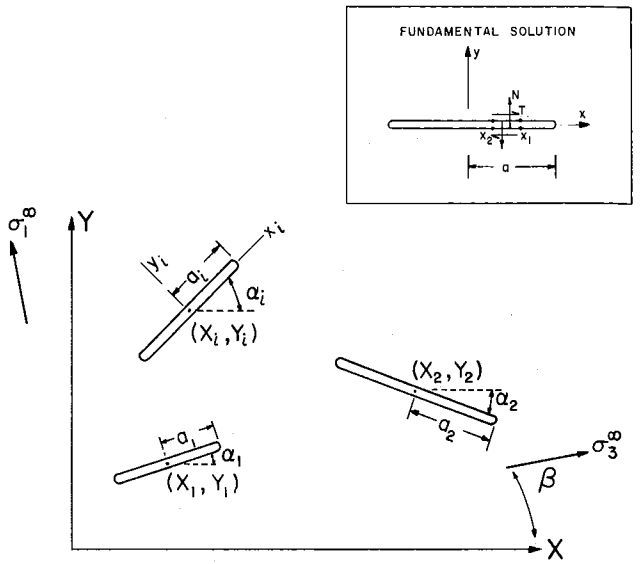

Fig. 4. Class of multiple-crack problems analyzed. An infinite elastic material containing any number of nonintersecting cracks is loaded by far-field principal stresses σ_1^∞ and σ_3^∞ oriented at an angle β with respect to a global coordinate (X, Y). Each crack is defined by coordinates of center point (X_i, Y_i), half-length a_i, and angle α_i that the crack makes with the X axis. Inset: fundamental solution used in the Schwarz-Neumann technique. Uniform normal (N) and shear (T) tractions are applied to crack between x_1 and x_2; remainder of crack is traction free.

found by *Pollard and Holzhausen* [1979], for an isolated crack having uniform tractions applied to part of the crack surface (Figure 4). Each crack surface is divided into a number of patches $n(i)$. Uniform normal (N) and shear (T) tractions act on opposing surfaces of the patch from $x(i)_1$ to $x(i)_2$, where x is position along the crack; the remainder of the crack is traction free, and all components of stress go to zero infinitely far from the crack. Adding the solutions for each patch together, we may approximate any arbitrary boundary condition on the crack surface. As the patch size decreases, a better approximation to a smoothly varying function is achieved. In order to economize on computation time and still maintain accuracy, we relate the patch size to stress gradients on the crack; that is, the patches are short where the resolved stress gradients are large and long where the stresses are nearly uniform.

An advantage of the Schwarz-Neumann technique is its flexibility: the number and orientation of the different cracks are unrestricted, providing the cracks do not intersect one another. Additionally, the boundary conditions on the crack surfaces are very general. For open (stress free) cracks the appropriate boundary conditions are $N = T = 0$, and for pressurized fluid-filled cracks, $N = -p$ and $T = 0$, where p is the internal pressure. The tractions need not be uniform but can be specified to satisfy the friction law $|T| \leq -f \cdot N$, where f is the coefficient of friction.

To illustrate the accuracy of the Schwarz-Neumann method, we compare our results with the exact solution for two collinear cracks subject to uniform tension [*Erdogan,* 1962]. Both cracks are of length $2a$, and their centers are separated by a distance $2b$. In Figure 5 we plot the opening mode stress intensity K_I at the inner crack tips, normalized by the value for a single crack K_I^0, versus the ratio a/b. As the cracks approach one another, K_I increases owing to the elastic interaction between cracks. Results computed for two different

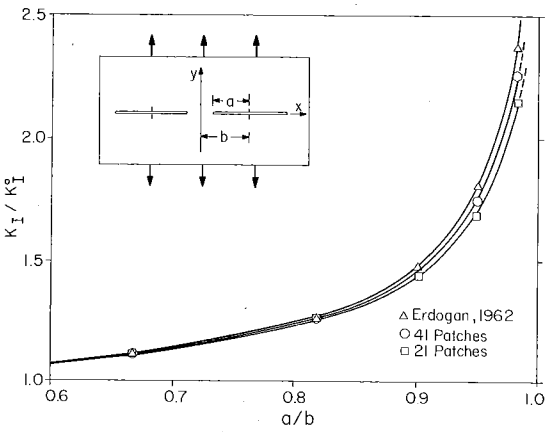

Fig. 5. Test of the Schwarz-Neumann technique, showing normalized mode I stress intensity K_I/K_I^0 at inner tips of two collinear cracks loaded in tension. Both cracks have half-length a and half-separation b. K_I^0 is the stress intensity at infinite separation. Computed results for two patch densities are compared with analytical solution derived by *Erdogan* [1962].

patch densities (n = 21 and 41) are plotted for comparison with the exact solution. The Schwarz-Neumann method is found to be accurate, even for a/b approaching 1.0. At a/b = 0.98 the calculated stress intensity is within 10% of the exact solution for n = 21 and within 5% for n = 41. An error of 10% is acceptable for the problems explored here. Other satisfactory comparisons were made with known solutions for single and multiple cracks.

Stresses Near Echelon Faults

In this section we investigate stress distributions near echelon cracks to provide some understanding of fault interaction for this important geometry. Although faults often consist of many individual segments arranged en echelon, we only consider the discontinuity between two segments, because the stresses in this region are dominated by the two closest segments. The stresses resulting from more distant segments are small in comparison. The geometry, applied stress, and frictional properties used in these examples (Figure 6) are meant not to apply to a particular field example, but to illustrate the character of the solution for geologically reasonable choices of parameters.

The step $2d$, or distance between cracks in the Y direction, is arbitrarily set at $d = +0.1a$ for left-stepping cracks and at $d = -0.1a$ for right-stepping cracks. The separation $2s$, or distance between crack tips in the X direction, is positive when the crack tips are apart, zero when they are both at $X = 0$, and negative when the tips overlap each other. In these examples the far-field stresses are both compressive with $\sigma_3^\infty = 5\sigma_1^\infty$, and the minimum compression σ_1^∞ is 60° from the X direction. The boundary conditions on the crack surfaces are specified to follow a linear friction law, in which the coefficient of friction f = 0.6. The normal component of traction N is continuous across the crack, and the shear component T satisfies the inequality $|T| \leq -f \cdot N$. In general, an additional condition on the crack displacements must be specified to insure opposite crack faces do not interpenetrate [*Dundurs and Comninou*, 1979]; in this analysis we specify that cracks remain closed.

Stress Distribution on Faults

For cracks parallel to the X axis the stress components that enter the boundary conditions are σ_{xy} and σ_{yy}. We can anticipate the nature of crack interaction from the σ_{xy} and σ_{yy} fields near a single crack subjected to unit pure shear in the far field (Figure 7). In regions where $\sigma_{xy} > 1$, the shear stress increase because of the crack, and in regions where $\sigma_{xy} < 1$ the shear stress decreases because of the presence of the crack (Figure 7*a*). Far from the crack, $\sigma_{xy} = 1$. An important feature of the σ_{yy} field (Figure 7*b*) is that the area around a single crack is divided into regions where $\sigma_{yy} > 0$ (tension) and regions where $\sigma_{yy} < 0$ (compression). Because the applied stress is pure shear, σ_{yy} approaches zero away from the crack.

Imagine inserting a second crack into the stress field of the single crack shown in Figure 7. If the step or separation is small in relation to the length of the two cracks, the interaction will be significant. If the inserted crack steps to the left, we see that for positive separation the inserted crack will undergo a small tension, σ_{yy}, normal to the crack faces and an increase in the shear stress σ_{xy}. If the separation is negative (crack tips overlap), the inserted crack will encounter a large compression across its tip that will tend to increase the frictional resistance to slip. In contrast, if the inserted crack steps to the right, the effects are reversed because of antisymmetry in the σ_{yy} distribution (Figure 7*b*). For a right step the inserted crack will undergo a small compression for positive separations but encounter a large tension at its tip for negative separations. This tension will reduce friction and facilitate slip near the end of the inserted crack.

Numerical solutions verify the conclusions drawn from examination of single-crack stress fields. For example, Figures 8*a* and 8*b* illustrate the distribution of normal and shear tractions on the right-hand crack of a right-stepping echelon pair with $d = -0.09a$ and $s = -0.09a$. The far-field stresses and boundary conditions are those specified at the beginning of this section. Interaction has reduced the compression $-N$ and the shear T by ~25% near the overlapped crack end. Plotting the frictional resistance $-f \cdot N$ and the shear T over the length of the crack in Figure 8*c*, it is evident that $-f \cdot N \approx T$, and so slip occurs everywhere on the crack. By contrast, for a pair of left-stepping cracks ($d = +0.09a$) the compression increases by ~25%, the shear stress decreases, and slip cannot occur near the overlapped crack tip. This result is quite general for right lateral shear and for separations smaller than the step. The in-

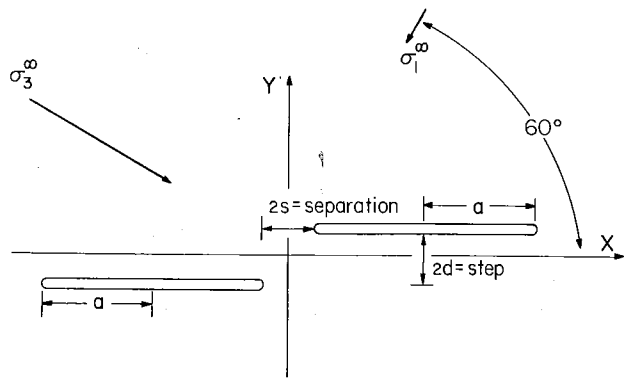

Fig. 6. Definitions of echelon crack geometry. Two cracks of half-length a are parallel to X direction; $2d$ is step between cracks, and $2s$ is separation between crack tips. Far-field stresses used in computations are also shown; $\sigma_3^\infty = 5\sigma_1^\infty$.

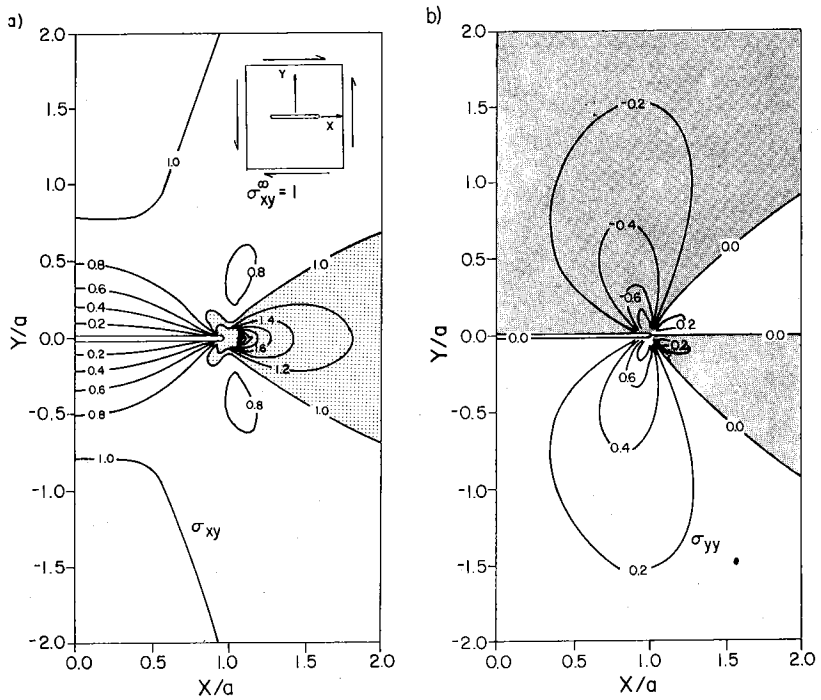

Fig. 7. Stress distribution around a single crack of unit half length, subjected to unit pure shear at infinity. (*a*) Shear stress σ_{xy} distribution. Because σ_{xy} is symmetrical about crack center ($x = 0$), the range of x is restricted to $0 \leq x \leq 2$. Shading denotes region where σ_{xy} increases significantly, owing to presence of crack. (*b*) Normal stress σ_{yy} distribution; σ_{yy} is antisymmetric about $x = 0$. Shading denotes regions where σ_{yy} is compressive.

teraction inhibits frictional sliding for left-stepping cracks and facilitates sliding for right-stepping cracks; this effect is reversed for left lateral shear.

Stress Distribution Between Fault Segments

The distribution of stress is markedly different in the region between two right-stepping and two left-stepping echelon cracks. To illustrate this contrast, we examine the stress distribution at small separation ($s/a = 0.06$) for both left- and right-stepping cracks. For left-stepping cracks this is the minimum separation that allows sliding to occur over the entire crack; smaller separation leads to sticking near the crack ends. Figure 9*a* illustrates the distribution of mean stress $\frac{1}{2}(\sigma_1 + \sigma_3)$ for left-stepping cracks. We note that the mean stress is everywhere compressive and that the compression increases to ~1.4 times the background value in the region between the cracks. In the region adjacent to, but outside, the cracks the mean stress is less than that in the far field. By contrast, the mean stress between two right-stepping cracks decreases to ~0.6 times the far-field value for the same applied stress (Figure 9*b*). A significant discontinuity exists in mean stress across the cracks in both cases. Figure 9*c* illustrates the distribution of maximum shear stress $\frac{1}{2}(\sigma_1 - \sigma_3)$ for left-stepping cracks. The increase in maximum shear is confined to the region between the cracks where it increases to ~1.4 times the background value. The region outside the cracks is subject to a decrease in maximum shear. By contrast, for right-stepping cracks the largest values of maximum shear occur in the regions outside the cracks (Figure 9*d*). Figures 9*c* and 9*d* also illustrate the orientation of σ_1, the minimum compression in the field. Far from the cracks, σ_1 is 60° from the X direction; any departures from this orientation are due to the presence of the cracks. For

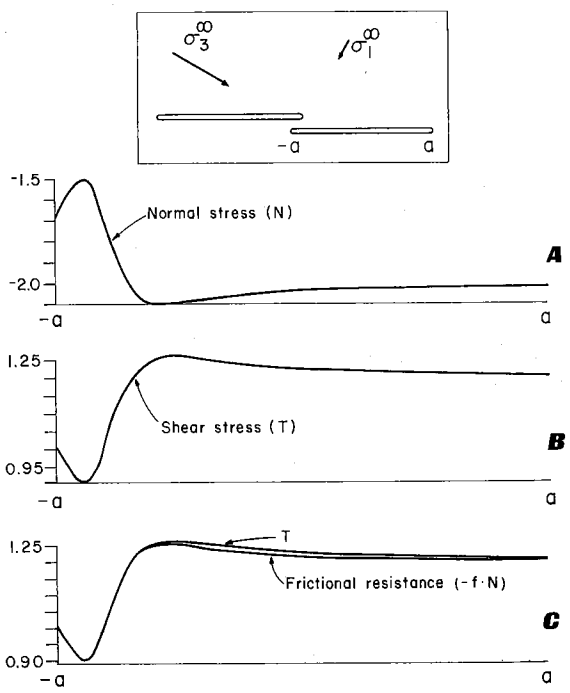

Fig. 8. Tractions acting on rightmost crack of a right-stepping echelon pair of cracks having $d/a = s/a = -0.09$. Applied stresses are same as in Figure 6. Inset: scale illustration of crack geometry, showing overlap and applied stress state. (*a*) Distribution of normal tractions N on right crack from $-a$ to a; negative values indicate compression. (*b*) Distribution of shear tractions T on right crack from $-a$ to a. (*c*) Replot of shear traction and frictional resistance ($-f \cdot N$) illustrating slip occurring over entire segment. Small discrepancy between the two curves is due to numerical error.

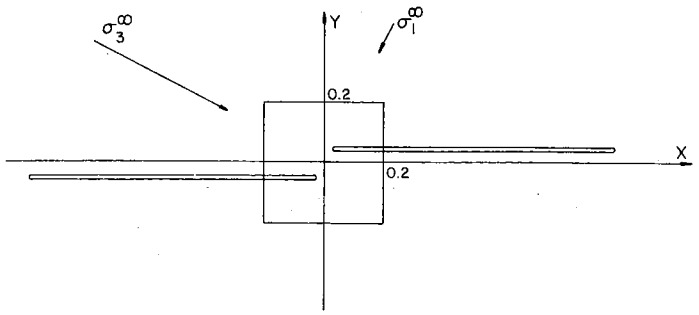

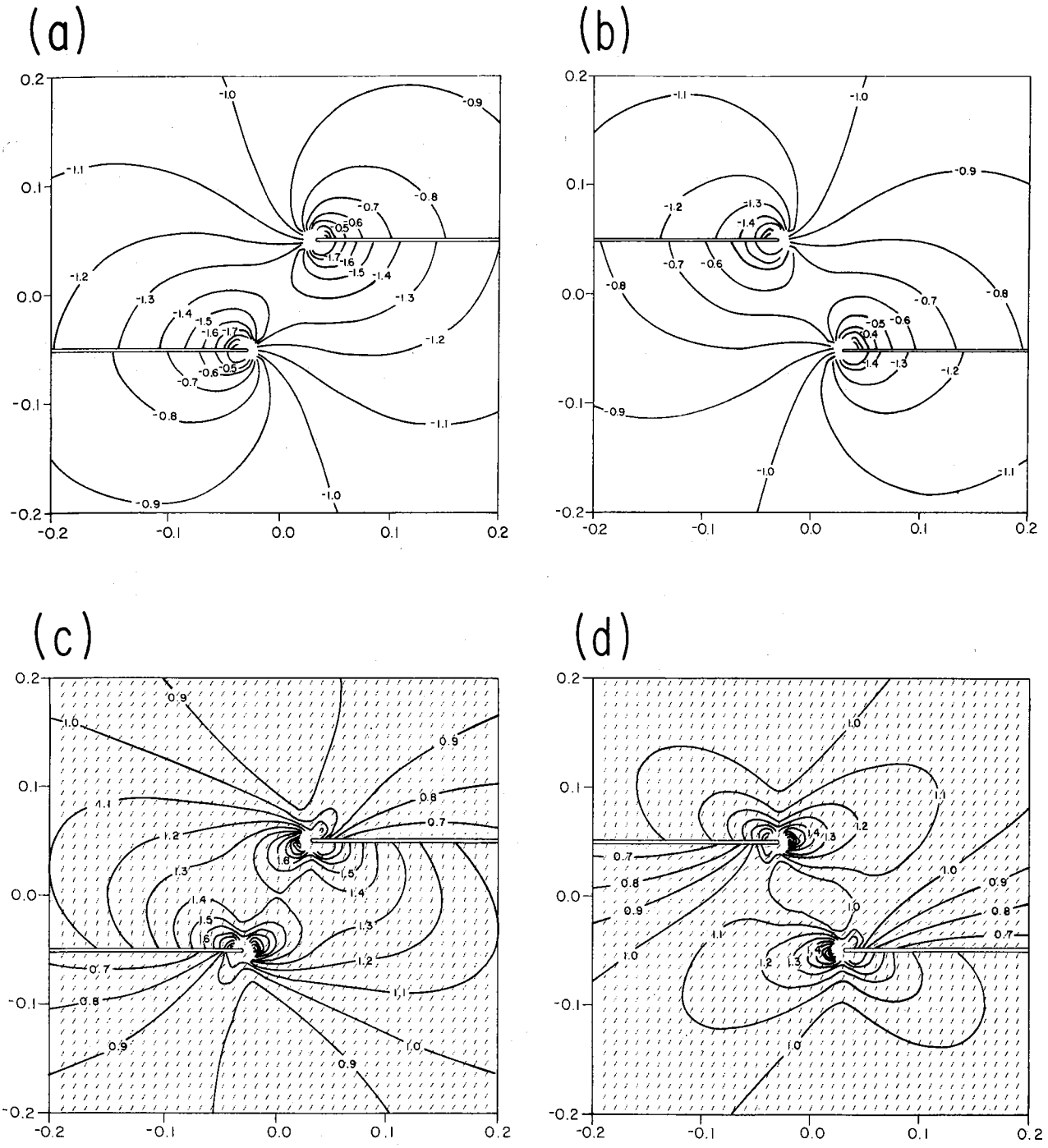

Fig. 9. State of stress near echelon discontinuities. Inset illustrates crack geometry, area plotted, and applied stress state. Distribution of mean stress $\frac{1}{2}(\sigma_1 + \sigma_3)$ for (*a*) left and (*b*) right step. Contoured values are normalized by far-field mean stress, so that background value is −1.0. Stresses <−1.0 represent an increase in confining pressure. Distribution of maximum shear stress $\frac{1}{2}(\sigma_1 - \sigma_3)$ for (*c*) left and (*d*) right step. Contoured values are normalized by the far-field maximum shear, so that background value is 1.0. Tick marks indicate direction of minimum compression σ_1. In the far field, σ_1 is 60° from the *X* direction.

left-stepping cracks, σ_1 is rotated counterclockwise by ~10° between the cracks, while for right-stepping cracks, σ_1 is rotated ~15° clockwise between the cracks. The principal stress directions are discontinuous across the crack planes. Discontinuities in stress orientation and magnitude at the crack are due to the discontinuity in σ_{xx} across the cracks.

Fault Discontinuity and Stress Drop

Following earthquakes that break the earth's surface, the relative displacement across the fault can be used in conjunction with the fault half length to infer the change in stress, or stress drop, during the event. For an isolated shear crack of half-length a undergoing a uniform stress change $\Delta\tau$ in a material of shear modulus μ,

$$\frac{\Delta\tau}{\mu} \simeq \frac{u_{\max}}{a} \tag{5}$$

where $u_{\max}$ is the maximum displacement on one side of the crack. *Aki* [1978] has pointed out that if fault segments behave as mechanically independent slipping surfaces, the observed displacement should be divided by the appropriate segment half length, not by the total fault half length. This approximation ignores elastic interaction of the segments that tends to increase the displacements for fixed segment lengths. Note that interaction leads to nonuniform stress changes on a given segment, as illustrated above (Figure 8).

To explore this result further, we calculate the maximum displacements for different numbers of segments n on a fault whose total length is fixed. The stresses and material properties are held constant, and so the variations in displacement depend solely on n. In this example, $s/a = 0$ and $a/d = 15$. In Figure 10 the ratio of maximum displacement to a characteristic length L is plotted against the number of segments n. In one set of calculations, L is taken to be the segment half-length a; in the second set, L is the total fault half-length na. The true stress change on the fault surfaces is the same for both calculations and for all values of n. Ignoring the interaction of different segments by choosing the segment half-length a as the appropriate length scale results in an overestimation of the stress change that increases as n increases. Conversely, treating the fault as a single crack by choosing the total fault half-length na as the appropriate length results in a significant underestimation of the stress change. For many elastically interacting segments, $u_{\max}/na$ is a poor estimate of the stress change on the fault surface. These results are only strictly appropriate when the deformation is entirely elastic. Significant fracturing between segments would tend to link adjacent segments, changing the effective lengths of the segments.

Secondary Fracturing

The large stresses predicted to exist in regions near closely spaced cracks may, under appropriate conditions, lead to secondary fracturing. Because the stress states for left- and right-stepping echelon cracks differ markedly, we expect that the style and extent of such fracturing might also differ. In experiments, two distinct styles of brittle failure have been recognized in rock [*Jaeger and Cook,* 1969, p. 86]: (1) extension failure—when the confining pressure is low, fractures cut the specimen and open perpendicular to the minimum compression (or maximum tension) σ_1; (2) shear failure—at larger confining pressures the two ends of the specimen slide along a

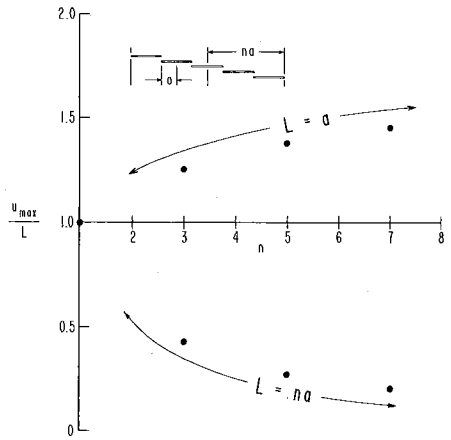

Fig. 10. Effect of number of fault segments on estimated stress change on the crack surface. Calculated maximum displacement $u_{\max}$ divided by segment half-length a (upper sequence of points) and total fault half-length na (lower sequence of points) is plotted versus the number of individual segments n.

plane or zone oriented at ≤45° to the maximum compression σ_3. We consider both styles of failure separately as mechanisms of secondary fracturing.

Extension failure is predicted when the local magnitude of maximum principal stress σ_1 equals the tensile strength. Because tensile strengths of rocks are small in magnitude, we approximate the boundary of the failure zone by the contour $\sigma_1 = 0$ (Figure 11). For left-stepping echelon cracks the area under tension is small and lies outside the cracks (Figure 11*a*). The stress orientation is such that extension fractures forming near the crack tips would propagate away from each other. For right-stepping cracks, under the same applied stresses, a much larger area of tension bridges the cracks (Figure 11*b*). Extension fractures forming near the crack tips would propagate into the region between the cracks.

The conditions for shear failure depend on both principal stresses σ_1 and σ_3 (or, equivalently, on the differential stress and confining pressure). A linear (Coulomb) relation between principal stresses at failure takes the form [*Jaeger and Cook,* 1969]

$$\sigma_1 = c_o + \sigma_3 \tan^2 (45° + \phi/2) \tag{6}$$

where c_o is the cohesion and ϕ is the internal friction angle. Rewriting (6) to conform with the tension-positive sign convention and defining $\tau = \frac{1}{2}(\sigma_1 - \sigma_3)$ and $\bar{\sigma} = \frac{1}{2}(\sigma_1 + \sigma_3)$, we find that a failure condition can be written as

$$F = a\tau + b\bar{\sigma} \tag{7}$$

where

$$a = \frac{1}{c_o}[1 + \tan^2 (45° + \phi/2)]$$

$$b = \frac{1}{c_o}[\tan^2 (45° + \phi/2) - 1]$$

Representative values of c_o and ϕ for granitic rocks are c_o = 2.3 kbar and $\phi = 33°$ [*Jaeger and Cook,* 1969], so that $a = 1.91$ and $b = -1.04$ (kbar). The material is predicted to fail on planes oriented by $45° - \phi/2$ (~30°) to the direction of maximum compression when $F = 1$ and not to fail when $F < 1$.

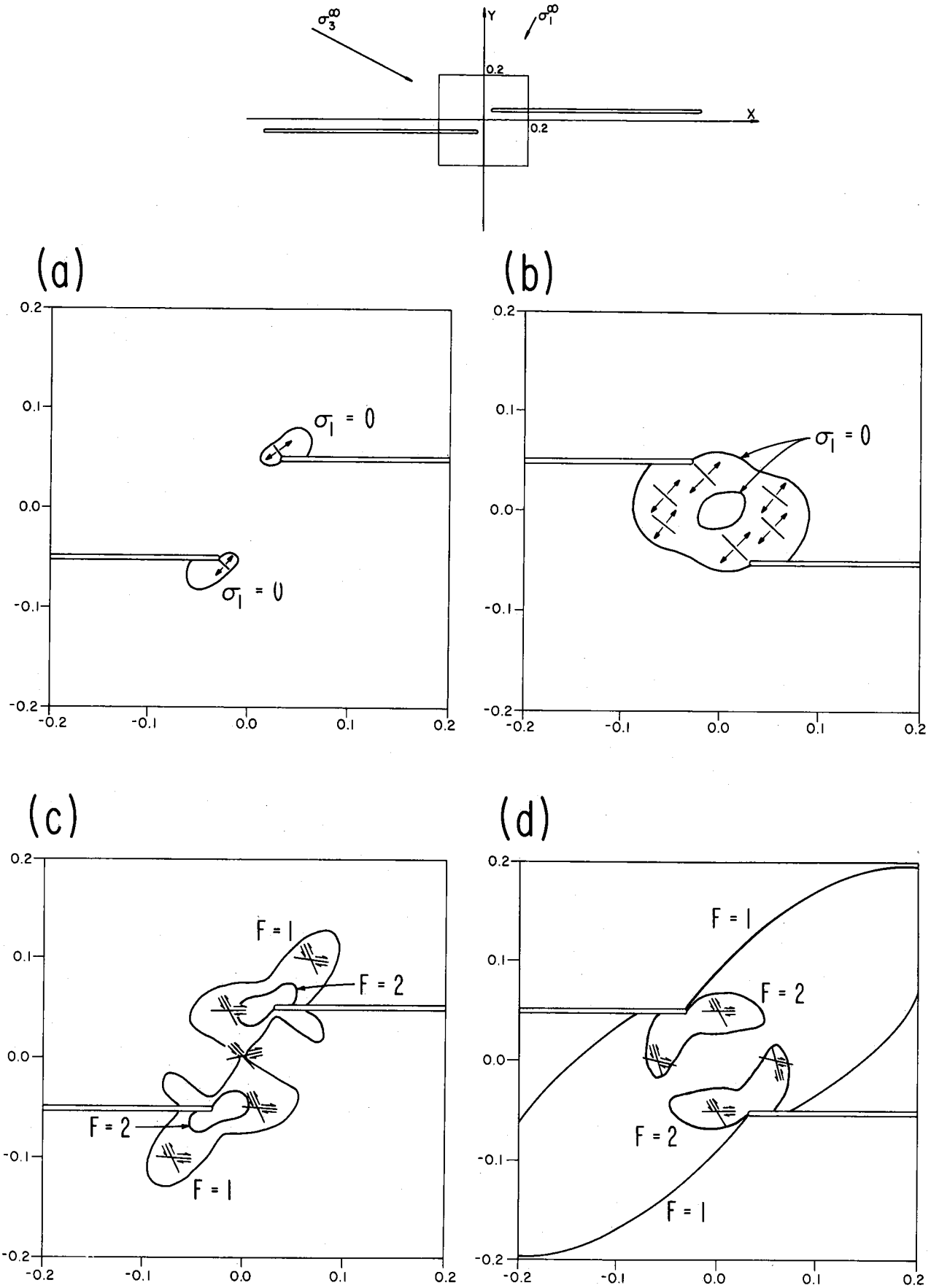

Fig. 11. Secondary fracturing near echelon discontinuities. Contour of the magnitude of maximum tension $\sigma_1 = 0$ for (*a*) left and (*b*) right step. Heavy contours enclose region of positive (tensile) stress and zone of potential tensile fracturing. Representative tensile fractures are drawn perpendicular to the local σ_1. Contour of shear failure condition F for (*c*) left and (*d*) right step. Illustrated contours are $F = 1.0$ and $F = 2.0$. Potential shear fractures are oriented at 30° to local maximum compression direction.

The contours $F = 1, 2$ are illustrated for both left- and right-stepping cracks in Figures 11*c* and 11*d*, respectively. For left-stepping cracks the shear-failure zone is restricted to the neighborhood of the crack tips. The zone of potential shear failure for right-stepping echelon cracks extends over a much wider area (Figure 11*d*).

We can draw several conclusions about secondary fracturing near echelon faults subject to right lateral shear. For left-stepping segments the following can be concluded: (1) short tensile cracks may form toward the outside of the step (Figure 11*a*), relieving the stress in this region and focusing any secondary shear fracturing ahead of, and between, the segments; (2) the line linking the segment ends is nearly perpendicular to the local maximum compression and is an unfavorable orientation for secondary fracture. Incipient shear fractures might form ahead of and parallel to the segments. The process would be stable, however, because the frictional resistance to slip would be great across the ends of the lengthened segments, as discussed above. The net effect may be that displacements decrease gradually toward the segment ends in such a way that the stress singularity is smoothed out and the echelon array is stabilized. If the driving stress is increased further, left lateral secondary shear fractures may form within the step oriented at about 60° to the lengthened segments (Figure 11*c*). For right-stepping segments the following can be concluded: (1) tensile fracturing may occur within the step (Figure 11*b*), possibly linking the segments and allowing slip to be transmitted through the step; the linked segments then act as a single segment of twice the original length, and so shear displacements may nearly double; (2) shear fracturing may occur within the step along planes as indicated in Figure 11*d*. Secondary normal faults forming in a right step between two vertical strike slip faults would strike in the same direction as the tensile cracks in Figure 11*b*.

Steeply dipping mining-induced normal faults in South Africa provide examples of secondary deformation associated with left steps. Secondary fractures were observed between left-stepping echelon fault segments [*Gay and Ortlepp,* 1979, Figure 6; *McGarr et al.,* 1979*a*, Figure 4]. The orientation and extent of fracturing is consistent with predictions based on the elastic model. Small tensile cracks formed toward the outside of the discontinuity (Figure 11*a*), and antithetic shear fractures formed between the segments (Figure 11*c*). More detailed modeling of this particular fault by *McGarr et al.* [1979*b*] yielded results similar to those presented here.

Small left lateral faults in the Sierra Nevada clearly illustrate the contrast in secondary fracturing associated with left and right steps [*Moore,* 1963]. Figure 12*a* illustrates a tensile fracture that bridged a left step, but not a smaller right step (compare with Figures 11*a* and 11*b*, recalling that left steps and left lateral shear are analogous to right steps when the shear is right lateral). In addition, small rhomb-shaped quartz-filled cavities commonly form between left steps [*Moore,* 1963]. If a tensile crack links two segments, further slip will be accommodated by opening of a rhombic cavity with opening equal to the slip transmitted through the step (Figure 12*b*).

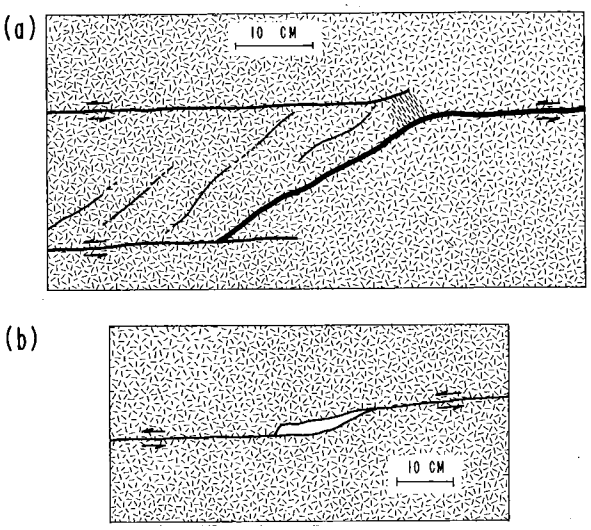

Fig. 12. Secondary fractures near steps in small left-lateral faults in granitic rocks of the Sierra Nevada. (*a*) Tensile fracture formed between left-stepping segments. A local foliation is developed between the right-stepping segments. (*b*) Small quartz-filled rhombic cavity in left step.

Constraints on Application of the Model

The results presented above were obtained for a two-dimensional (plane strain or plane stress) solution to an elastic problem in which crack geometry, boundary conditions, and deformation vary only in the XY plane. Consider the following potential deviations from this simple description: (1) the presence of a nearby free surface, (2) finite deformations associated with many episodes of fault slip, (3) inelastic deformation between closely spaced segment ends, (4) variations in the state of stress with depth, and (5) changes in the geometric arrangement or number of segments with depth.

The plane strain analysis applies to a fault with dimension in Z that is large in relation to the half-length a measured in the XY plane. This analysis is also applicable to a buried fault if the depth h to the fault is large in relation to a. We estimate a limit for h/a from the critical radius r_c/a defined earlier. Creating a free surface beyond the critical radius by removing the small stresses acting on the surface has little effect on the fault. Thus a buried fault is not significantly affected by the earth's surface if $h/a > 3$.

Near the earth's surface the stress state is approximated by plane stress conditions, and our analysis is applicable if the XY plane is horizontal and the fault intersects the surface. Because strain in Z is proportional to the mean stress in the XY plane for plane stress [*Timoshenko and Goodier,* 1951, p. 142], we expect the distribution of vertical displacements in the horizontal plane to correlate with the mean stress distribution. This is corroborated by inspection of vertical displacements and mean stress at the surface of a semiinfinite body containing a crack in shear [*Chinnery,* 1961, 1963]. For right lateral shear and a left step the mean stress increases between echelon faults (Figure 9*a*), corresponding to surface uplift. The mean stress decreases between faults at a right step (Figure 9*b*), corresponding to surface downwarp. This conclusion is similar to that of *Rodgers* [1980] and compares qualitatively well with deformation at the Ocotillo Badlands (Figure 1) and Mesquite Lake (Figure 2). At these localities, trends of fold axes and normal faults, which are taken to represent principal directions, are consistent with the elastic analysis. Of course, the deformation at these localities has accumulated over many individual slip events, and the total strains are clearly finite and largely inelastic. In addition, processes of erosion and deposition have modified the surfaces. The correlation between observations and theory implies that each increment of

deformation and uplift has been dominated by slip on fault segments with the present geometry.

If inelastic deformation allows significant slip to be transmitted through an echelon step, then a single crack, equal in length to the two segments, better approximates the elastic fields away from the step. If the rock within a step is largely intact, failure at the low confining pressures of the upper crust is by brittle fracture as considered above. If fractured rock or gouge predominates, deformation may occur as distributed plastic flow. We estimate the importance of plastic yielding between segment ends, by comparing the size of the plastic zone for a single segment with typical spacings between segments. Yielding of a perfectly plastic material at the tip of a mode III crack occurs in a circular zone of radius R. The stress field in the elastic region is determined by the purely elastic solution for a crack of half-length $a + R$, that is, one in which the actual crack tip is moved ahead to the center of the plastic zone [*Rice,* 1968]. The size of the plastic zone is estimated by $R/a = \frac{1}{2}(\sigma^a/\tau_y)^2$, where σ^a is the applied shear stress and τ_y is the plastic yield strength. This approximation is valid for $\sigma^a/\tau_y \leq 0.5$. In order for plastic yield to spread between adjacent segments, $R/a = d/a$, where d is the half step between fault segments. Measuring d/a for the Coyote Creek, San Andreas (near Parkfield), and Imperial-Brawley fault steps (Figures 1, 14, and 2), we find $d/a = 1/20$–$1/10$. For plastic yield to extend between the segments, $\sigma^a/\tau_y = (2d/a)^{1/2} = 0.3$–$0.4$. Applied shear stress in the upper crust is of the order of 100 bars [*McGarr and Gay,* 1978], while yield strengths range from 1 kbar for some natural fault gouges [*Logan et al.,* 1979] to as low as 100–200 bars for pure water-saturated clay [*Wang and Mao,* 1979]. Comparison with fault zones exposed in mines suggests that clayey gouge comprises a small fraction of the fault zone [*Wallace and Morris,* 1979]. Thus it appears that $\sigma^a/\tau_y < 0.1$, although it could be greater in some instances. Hence for faulting in the upper crust it appears that inelastic deformation between segment ends is more likely to occur as brittle fracturing than as plastic deformation.

The effect of increasing confining pressure with depth can be approximated using the two-dimensional solution by choosing applied stresses appropriate for different depths. Large confining pressures stabilize rock to both extension and shear failure. Thus changing the ratio of mean stress to maximum shear stress will alter the size and shape of the failure zones in Figure 11.

To assess the value of a two-dimensional solution in studying faults, the changes in fault geometry with depth must be known; however, little, if anything, is known about the three-dimensional form of faults. Because adjacent ends of echelon fault segments often dip toward one another, several workers [*Clayton,* 1966, Figure 4; *Sharp and Clark,* 1972, Figure 94] suggest that segments coalesce into a single fault at depth, as illustrated in Figure 13. If this geometry is appropriate, then the ratio l/c (where l is the depth at which the faults coalesce and c is the total fault depth in the Z direction) determines the character of deformation in the XY plane. As l/c approaches 1, the deformation is adequately approximated by a two-dimensional solution for n nonintersecting segments of half-length a. As l/c approaches zero, surface deformation would be better described by a single fault of length na. The character of surface deformation also depends on the distance x from the fault. For small x/a the deformation is greatly influenced by fault segments extending from the surface to $Z = l$. For large x/a, however, the deformation is approximated by a single fault of length na and depth c. The proper geometry is thus chosen by considering the individual fault segments for large l/c and/or small x/a and by ignoring discontinuities and treating the fault as a single surface for small l/c and/or large x/a. For intermediate values of l/c and x/a the problem is inherently three dimensional. The appropriate choice of model geometry depends strongly on the depth of convergence (l/c), which at present must be evaluated for each individual fault.

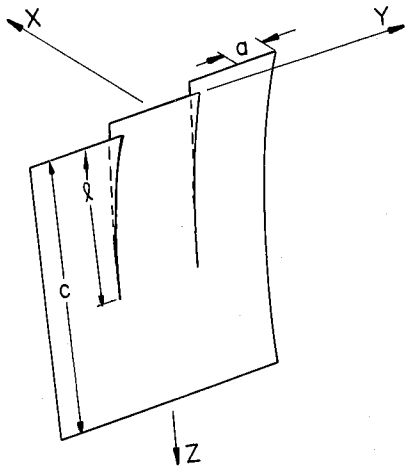

Fig. 13. Schematic illustration of possible fault geometry in three dimensions. Fault segments of half-length a intersect the XY plane and coalesce into a single fault at depth l; fault plane extends to total depth c.

Seismicity Associated With Fault Discontinuities

Studies of earthquake source mechanics require that the faulting process be heterogeneous at length scales small in comparison with the rupture length [*Hanks,* 1979; *Nur,* 1978; *Andrews,* 1980]. As discussed by *Nur* [1978], heterogeneities on many length scales are necessary to explain important features of the faulting process. In this light, it is interesting to note that irregularities in fault geometry occur at many length scales, give rise to significant local stresses (Figures 7, 8, and 9), and may therefore be important in creating and maintaining heterogeneous stresses on faults.

Recent studies of detailed seismicity have demonstrated that earthquakes tend to cluster near steps and other irregularities along some faults [*Bakun et al.,* 1980]. A particularly well studied event in which fault geometry evidently influenced seismicity was the 1966 Parkfield-Cholame, California, earthquake (Figure 14). Two separate aspects of the local fault geometry are important. *Lindh and Boore* [1974] reported that the epicenter of the magnitude 5.5 main event was located near a 5° bend in the fault trace; a magnitude 5.1 foreshock was located ~1 km to the northwest. *Bakun and McEvilly* [1979] inferred that rupture of the foreshock propagated to the northwest, but rupture of the main shock propagated to the southeast. While we have not explicitly considered the effect of small changes in fault strike, we can draw some conclusions about the interaction in this case. Slip northwest of the epicenter, in the form of both foreshocks and aseismic creep, increased the shear stress acting on the central fault segment. Because of the slight change in strike, a change in normal stress would also occur. We can judge the sign of the normal stress change by treating the northern segment as a single

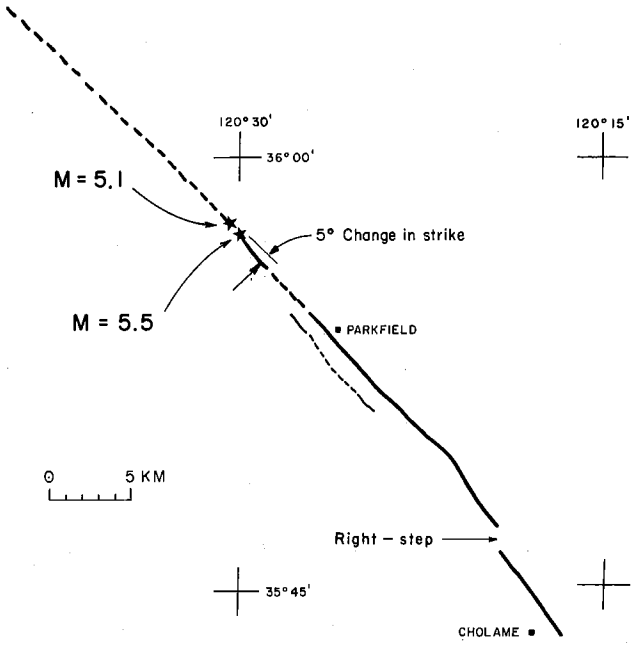

Fig. 14. San Andreas fault near Parkfield, California. Solid lines indicate observed ground breakage during the 1966 event; dashed lines indicate the inferred trace of the fault [*Brown*, 1970]. The largest ($M = 5.1$) foreshock and the $M = 5.5$ main shock are also shown [after *McEvilly et al.*, 1967].

shear crack. We make use of the near-tip approximation for the stresses, expressed in an (r, θ) coordinate system centered on the crack tip [*Rice*, 1968]. Here it is considered positive for angles measured counterclockwise from a line coincident with the extension of the crack. For a given applied stress and distance from the crack tip, the normal stress $\sigma_{\theta\theta}$ is

$$\sigma_{\theta\theta} \propto -3 \cos^2 (\theta/2) \sin (\theta/2) \qquad (8)$$

or, for small θ, $\sigma_{\theta\theta} \propto -3\theta/2$. For slip north of the bend, $\theta = -5°$ (Figure 14). Thus slip north of the epicenter adds a small tension across the central segment and reduces the frictional resistance to slip. The large foreshock to the north of the epicenter destabilized the fault to the south and may have triggered the main shock. Interestingly, for coseismic slip on the central segment, $\theta = +5°$ and the induced normal stress north of the bend is compressive. The increased compression, which inhibits slip, may help to explain the paucity of aftershocks north of the bend.

The second point of interest is the pronounced 1-km right step in the fault, which can be seen both in the surface trace [*Brown*, 1970] and in the aftershock distribution [*Eaton et al.*, 1970]. For right lateral shear, right-stepping offsets are sites of reduced frictional resistance to slip and of increased potential for secondary fracturing. Thus we might expect right steps to be areas of concentrated aftershock activity. This was indeed true for the Parkfield aftershock sequence [*Eaton et al.*, 1970]. The cumulative aftershock slip near the step was more than twice that anywhere else in the aftershock zone [*Lindh and Boore*, 1980]; precisely at this step the surface slip was zero. These observations suggest that aftershocks occurred on many distributed fractures concentrated near the step, or possibly as adjustment of the adjacent segment ends where the interaction is strongest (recall Figure 8).

Additional examples of increased seismicity near right steps in right lateral faults have been described previously [*Hill*, 1977; *Weaver and Hill*, 1978/1979]. The right step between the Brawley and Imperial faults, described above, is of this type. Earthquake swarms in the Imperial Valley occurred along the Imperial and Brawley faults with epicenters clustering either on the two main faults near the step or in the region between the offset faults [*Johnson and Hadley*, 1976; *Johnson*, 1979]. Individual swarms were localized on trends transverse to the main faults. Swarms initiated on the main faults but in time developed progressively away from them. *Johnson* [1979] has interpreted this behavior as the growth of secondary faults. Fault plane solutions associated with the main faults were dominantly strike slip, whereas those associated with secondary faults were both strike slip and dip slip. Aftershocks of the 1979 El Centro earthquake are strongly clustered near the right step with the Brawley fault [*Johnson and Hutton*, 1980]. The character of seismicity in the Imperial Valley is compatible with our general conclusions concerning slip and secondary fracturing associated with right steps. According to this interpretation, secondary fracturing is due to the stress state produced by slip on the main faults. The reduced mean stress associated with right steps (Figure 9*b*) would also favor dike intrusion in these regions, and indeed the high heat flows and geothermal phenomena in at least a few right steps suggest igneous activity [*Weaver and Hill*, 1978/1979].

SUMMARY

Fault traces exhibit complex geometries which may be approximated as arrays of echelon segments. For a given sense of shear, left- and right-stepping pairs of fault segments have pronounced differences in mechanical behavior exemplified by the static stress and deformation fields near echelon cracks in an elastic material. Small changes in either the segment length or the step greatly alter the response of the segments to loading. Through elastic interaction, simultaneous slip on adjacent segments may locally enhance or impede further slip. This important result is not found in solutions where the stress fields surrounding adjacent cracks are simply superimposed. Confidence in application of the crack model to faults is gained through comparison with the following: (1) predicted distribution and orientation of secondary fractures near echelon steps correlate well with those observed in the Sierra Nevada and in South African mines; (2) deformation and vertical displacements are consistent with observations at steps in major strike slip faults in California.

We conclude that accurate maps of fault geometry are an important requirement in understanding faulting. Furthermore, one must know how to extrapolate surface geometry to seismogenic depths. Examples such as the 1966 Parkfield aftershock sequence indicate that ~1-km steps extend to depths of 10 km. However, we do not know if such extrapolations are warranted in general. Measurements of surface deformation and seismicity near steps should clarify this point and provide valuable information about the transfer of slip between segments. If surface offsets extend to seismogenic depth along right lateral faults, right steps may be sites of swarm seismicity and aftershocks, while left steps may store strain and may be sites of larger earthquakes.

Acknowledgments. Many examples of deformation and seismicity associated with fault discontinuities were brought to our attention by colleagues at the U.S. Geological Survey. We particularly wish to thank D. J. Andrews, W. H. Bakun, P. T. Delaney, D. P. Hill, A. Lindh, G. M. Mavko, A. McGarr, and R. V. Sharp. An early draft of

the manuscript was critically reviewed by W. H. Bakun, A. M. Johnson, and A. McGarr. One of the authors (P.S.) was supported by a National Science Foundation graduate fellowship during early stages of the research.

REFERENCES

Aki, K., A quantitative model of stress in a seismic region as a basis for earthquake prediction, in *Proceedings of Conference III: Fault Mechanics and Its Relation to Earthquake Prediction, Open File Rep. 78-380,* pp. 7–13, U.S. Geological Survey, Menlo Park, Calif., 1978.

Allen, C. R., Active faulting in northern Turkey, *Contrib. 1577,* 32 pp., Div. of Geol. Sci., Calif. Inst. of Technol., Pasadena, 1968.

Andrews, D. J., A stochastic fault model, *J. Geophys. Res.,* in press, 1980.

Aydin, A., Faulting in sandstone, Ph.D. thesis, 246 pp., Stanford Univ., Stanford, Calif., 1977.

Bakun, W. H., and T. V. McEvilly, Earthquakes near Parkfield, California: Comparing the 1934 and 1966 sequence, *Science, 205,* 1375–1377, 1979.

Bakun, W. H., R. M. Stewart, C. G. Bufe, and S. M. Marks, Implication of seismicity for failure of a section of the San Andreas fault, *Bull. Seismol. Soc. Amer., 70,* 185–201, 1980.

Bonilla, M. G., Historic faulting-map patterns, relation to subsurface faulting, and relation to pre-existing faults, in *Proceedings of Conference VIII: Analysis of Actual Fault Zones in Bedrock, Open File Rep. 79-1239,* pp. 36–65, U.S. Geological Survey, Menlo Park, Calif., 1979.

Brady, B. T., Theory of earthquakes, II, Inclusion theory of crustal earthquakes, *Pure Appl. Geophys., 113,* 149–168, 1975.

Brown, R. D., Map showing recently active breaks along the San Andreas fault between the northern Gabilan Range and Cholame Valley, California, *U.S. Geol. Surv. Misc. Geol. Inv. Map, 1-575,* scale 1:62,500, 1970.

Chinnery, M. A., The deformation of the ground around surface faults, *Bull. Seismol. Soc. Amer., 51,* 355–372, 1961.

Chinnery, M. A., The stress changes that accompany strike-slip faulting, *Bull. Seismol. Soc. Amer., 53,* 921–932, 1963.

Chinnery, M. A., Theoretical fault models, in *A Symposium on Processes in the Focal Region,* Dominion Observatory, Ottawa, 1968.

Clark, M. M., Surface rupture along the Coyote Creek fault, *U.S. Geol. Surv. Prof. Pap., 787,* 55–86, 1972.

Clark, M. M., Map showing recently active breaks along the Garlock and associated faults, California, *U.S. Geol. Surv. Misc. Geol. Inv. Map, I-741,* scale 1:24,000, 1973.

Clayton, L., Tectonic depressions along the Hase fault, a transcurrent fault in north Canterbury, New Zealand, *N. Z. J. Geol. Geophys., 9,* 94–104, 1966.

Delameter, W. R., G. Herrmann, and D. M. Barnett, Weakening of an elastic solid by a rectangular array of cracks, *J. Appl. Mech., 42,* 74–80, 1975.

Dewey, J. W., Seismicity of northern Anatolia, *Bull. Seismol. Soc. Amer., 66,* 843–868, 1976.

Dieterich, J. H., Preseismic fault slip and earthquake prediction, *J. Geophys. Res., 83,* 3940–3948, 1978.

Dundurs, J., and M. Comninou, The interface crack in retrospect and prospect, in *Fracture of Composite Materials,* edited by G. C. Sih and V. P. Tamuzs, pp. 93–107, Sithoff and Noordhoff, Leyden, the Netherlands, 1979.

Eaton, J. P., M. E. O'Neill, and J. N. Murdock, Aftershocks of the 1966 Parkfield-Cholame, California, earthquake: A detailed study, *Bull. Seismol. Soc. Amer., 60,* 1151–1197, 1970.

Erdogan, F., On the stress distribution in plates with collinear cuts under arbitrary loads, in *Proceedings of the 4th U.S. National Congress on Applied Mechanics,* vol. 1, pp. 547–553, American Society of Mechanical Engineers, New York, 1962.

Gay, N. C., and W. D. Ortlepp, Anatomy of a mining-induced fault zone, *Geol. Soc. Amer. Bull., 90,* 47–58, 1979.

Hanks, T. C., Earthquake stress drops, ambient tectonic stress, and stresses that drive plate motions, *Pure Appl. Geophys., 115,* 441–458, 1977. (Also *Geol. Soc. Amer. Bull., 90,* 47–58, 1979.)

Hanks, T. C., *b* values and *w* seismic source models, *J. Geophys. Res., 84,* 2235–2242, 1979.

Hill, D. P., A model for earthquake swarms, *J. Geophys. Res., 82,* 1347–1352, 1977.

Ishida, M., Method of Laurent series expansion for internal crack problems, in *Mechanics of Fracture 1: Methods of Analysis and Solutions of Crack Problems,* edited by G. C. Sih, pp. 56–130, Sithoff and Noordhoff, Leyden, the Netherlands, 1973.

Jaeger, J. C., and N. G. Cook, *Fundamentals of Rock Mechanics,* 513 pp., Methuen, London, 1969.

Johnson, C. E., Seismotectonics of the Imperial Valley of southern California, Ph.D. thesis, Calif. Inst. of Technol., Pasadena, 1979.

Johnson, C. E., and D. M. Hadley, Tectonic implications of the Brawley earthquake swarm, Imperial Valley, California, January, 1975, *Bull. Seismol. Soc. Amer., 66,* 1132–1144, 1976.

Johnson, C. E., and L. K. Hutton, The 15 October 1979 Imperial Valley earthquake: A study of aftershocks and prior seismicity, in *The Imperial Valley, CA, Earthquake of Oct. 15, 1979,* edited by C. E. Johnson, C. Rojahn, and R. V. Sharp, U.S. Geological Survey, Reston, Va., in press, 1980.

Koiter, W. T., An infinite row of parallel cracks in an infinite elastic sheet, in *Problems of Continuum Mechanics,* edited by J. R. M. Radok, Society for Industrial and Applied Mathematics, Philadelphia, Pa., 1961.

Kranz, R. L., Crack-crack and crack-pore interactions in stressed granite, *Int. J. Rock Mech. Min. Sci. Geomech. Abstr., 16,* 37–47, 1979.

Lachenbruch, A. H., and J. H. Sass, Thermomechanical aspects of the San Andreas Fault system, in *Proceedings of the Conference on Tectonic Problems of the San Andreas Fault System,* edited by R. L. Kovach and A. Nur, School of Earth Sciences, Stanford University, Stanford, Calif., 1973.

Lindh, A., and D. M. Boore, The relation of the Parkfield foreshocks to the initiation and extent of rupture, *Earthquake Notes, 45,* 54, 1974.

Lindh, A., and D. M. Boore, Control of rupture by fault geometry during the 1966 Parkfield earthquake, submitted to *Bull. Seismol. Soc. Amer.,* 1980.

Logan, J. M., N. Higgs, M. Friedman, and H. Gato-Bauer, Preliminary investigation of core material from U.S.G.S. Dry Valley no. 1 well, San Andreas Fault (abstract), *Eos Trans. AGU, 60,* 956, 1979.

McEvilly, T. V., W. H. Bakun, and K. B. Casaday, The Parkfield, California earthquake of 1966, *Bull. Seismol. Soc. Amer., 57,* 1221–1244, 1967.

McGarr, A., and N. C. Gay, State of stress in the earth's crust, *Annu. Rev. Earth Planet. Sci., 6,* 405–436, 1978.

McGarr, A., S. M. Spottiswode, N. C. Gay, and W. D. Ortlepp, Observations relevant to seismic driving stress, stress drop, and efficiency, *J. Geophys. Res., 84,* 2251–2261, 1979*a*.

McGarr, A., D. D. Pollard, N. C. Gay, and W. D. Ortlepp, Observations and analysis of structures in exhumed mine-induced faults, in *Proceedings of Conference VIII: Analysis of Actual Fault Zones in Bedrock, Open File Rep. 79-1239,* pp. 101–120, U.S. Geological Survey, Menlo Park, Calif., 1979*b*.

Moore, J. G., Geology of the Mount Pinchot quadrangle, southern Sierra Nevada, California, *U.S. Geol. Surv. Bull., 1130,* 152, 1963.

Muskhelishvili, N. I., *Some Basic Problems of the Mathematical Theory of Elasticity,* P. Noordhoff Ltd., Groningen, The Netherlands, 1954.

Nur, A., Nonuniform friction as a physical basis for earthquake mechanics, *Pure Appl. Geophys., 116,* 964–991, 1978.

Paris, P., and G. Sih, Stress analysis of cracks, in *Symposium on Fracture Toughness Testing and Applications, Spec. Tech. Publ. 381,* pp. 30–81, American Society for Testing and Materials, Philadelphia, Pa., 1965.

Pollard, D. D., and G. Holzhausen, On the mechanical interaction between a fluid-filled fracture and the earth's surface, *Tectonophysics, 53,* 27–57, 1979.

Pucik, T. A., Elastostatic interaction of cracks in the infinite plane, Ph.D. thesis, Calif. Inst. of Technol., Pasadena, 1972.

Rice, J. R., Mathematical analysis in the mechanics of fracture, in *Fracture: An Advanced Treatise,* vol. II, edited by H. Liebowitz, pp. 191–311, Academic, New York, 1968.

Rodgers, D. A., Analysis of basin development produced by en echelon strike slip faults, in *Sedimentation at Oblique-Slip Margins, Spec. Publ. 4,* edited by P. F. Ballance and H. G. Reading, International Association of Sedimentologists, Oxford, England, in press, 1980.

Rudnicki, J. W., The inception of faulting in a rock mass with a weakened zone, *J. Geophys. Res., 82,* 844–854, 1977.

Sharp, R. V., Map showing recently active breaks along the San Jacinto fault zones between the San Bernardino area and Borrego

Valley, California, *U.S. Geol. Surv. Misc. Geol. Inv. Map, I-675,* scale 1:24,000, 1972.
Sharp, R. V., Surface faulting in Imperial Valley during the earthquake swarm of January–February 1975, *Bull. Seismol. Soc. Amer., 66,* 1145–1154, 1976.
Sharp, R. V., and M. M. Clark, Geologic evidence of previous faulting near the 1968 rupture on the Coyote Creek fault, *U.S. Geol. Surv. Prof. Pap., 787,* 131–140, 1972.
Sokolnikoff, I. S., *Mathematical Theory of Elasticity,* 2nd ed., 475 pp., McGraw-Hill, New York, 1956.
Stuart, W. D., Strain softening prior to two-dimensional strike-slip earthquakes, *J. Geophys. Res., 84,* 1063–1070, 1979.
Stuart, W. D., and G. M. Mavko, Earthquake instability on a strike-slip fault, *J. Geophys. Res., 84,* 2153–2160, 1979.
Tchalenko, J. S., and N. N. Ambraseys, Structural analysis of the Dasht-e Bayaz (Iran) earthquake fractures, *Geol. Soc. Amer. Bull., 81,* 41–60, 1970.
Timoshenko, S., and J. N. Goodier, *Theory of Elasticity,* 506 pp., McGraw-Hill, New York, 1951.
Vedder, J. G., and R. E. Wallace, Map showing recently active breaks along the San Andreas and related faults between Cholame Valley and Tejon Pass, California, *U.S. Geol. Surv. Misc. Geol. Inv. Map, I-574,* scale 1:24,000, 1970.
Wallace, R. E., Surface fracture patterns along the San Andreas Fault, in *Proceedings of the Conference on Tectonic Problems of the San Andreas Fault System,* edited by R. L. Kovach and A. Nur, School of Earth Sciences, Stanford University, Stanford, Calif., 1973.
Wallace, R. E., and H. T. Morris, Characteristics of faults and shear zones in mines at depths as much as 2.5 km below the surface, in *Proceedings of Conference VIII: Analysis of Actual Fault Zones in Bedrock, Open File Rep. 79-1239,* pp. 79–100, U.S. Geological Survey, Menlo Park, Calif., 1979.
Wang, C., and N. Mao, Shearing of saturated clays in rock joints at high confining pressures, *Geophys. Res. Lett., 6,* 825–828, 1979.
Weaver, C. S., and D. P. Hill, Earthquake swarms and local crustal spreading along major strike-slip faults in California, *Pure Appl. Geophys., 117,* 51–64, 1978/1979.
Weertman, J., Relationship between displacement on a free surface and the stress on a fault, *Bull. Seismol. Soc. Amer., 55,* 945–953, 1965.
Yokobori, T. M. Uozumi, and M. Ichikawa, Interaction between non-coplanar parallel staggered elastic cracks, in *Rep. Inst. Strength and Fracture of Materials, 7,* 25–47, Tohoku University, 1971.
Zoback, M. D., and J. C. Roller, Magnitude of shear stress on the San Andreas Fault: Implications of a stress measurement profile at shallow depth, *Science, 206,* 445–447, 1979.

(Received November 7, 1979;
accepted January 9, 1980.)

left-stepping cracks, σ_1 is rotated counterclockwise by ~10° between the cracks, while for right-stepping cracks, σ_1 is rotated ~15° clockwise between the cracks. The principal stress directions are discontinuous across the crack planes. Discontinuities in stress orientation and magnitude at the crack are due to the discontinuity in σ_{xx} across the cracks.

Fault Discontinuity and Stress Drop

Following earthquakes that break the earth's surface, the relative displacement across the fault can be used in conjunction with the fault half length to infer the change in stress, or stress drop, during the event. For an isolated shear crack of half-length a undergoing a uniform stress change $\Delta\tau$ in a material of shear modulus μ,

$$\frac{\Delta\tau}{\mu} \simeq \frac{u_{\max}}{a} \tag{5}$$

where $u_{\max}$ is the maximum displacement on one side of the crack. *Aki* [1978] has pointed out that if fault segments behave as mechanically independent slipping surfaces, the observed displacement should be divided by the appropriate segment half length, not by the total fault half length. This approximation ignores elastic interaction of the segments that tends to increase the displacements for fixed segment lengths. Note that interaction leads to nonuniform stress changes on a given segment, as illustrated above (Figure 8).

To explore this result further, we calculate the maximum displacements for different numbers of segments n on a fault whose total length is fixed. The stresses and material properties are held constant, and so the variations in displacement depend solely on n. In this example, $s/a = 0$ and $a/d = 15$. In Figure 10 the ratio of maximum displacement to a characteristic length L is plotted against the number of segments n. In one set of calculations, L is taken to be the segment half-length a; in the second set, L is the total fault half-length na. The true stress change on the fault surfaces is the same for both calculations and for all values of n. Ignoring the interaction of different segments by choosing the segment half-length a as the appropriate length scale results in an overestimation of the stress change that increases as n increases. Conversely, treating the fault as a single crack by choosing the total fault half-length na as the appropriate length results in a significant underestimation of the stress change. For many elastically interacting segments, $u_{\max}/na$ is a poor estimate of the stress change on the fault surface. These results are only strictly appropriate when the deformation is entirely elastic. Significant fracturing between segments would tend to link adjacent segments, changing the effective lengths of the segments.

Secondary Fracturing

The large stresses predicted to exist in regions near closely spaced cracks may, under appropriate conditions, lead to secondary fracturing. Because the stress states for left- and right-stepping echelon cracks differ markedly, we expect that the style and extent of such fracturing might also differ. In experiments, two distinct styles of brittle failure have been recognized in rock [*Jaeger and Cook*, 1969, p. 86]: (1) extension failure—when the confining pressure is low, fractures cut the specimen and open perpendicular to the minimum compression (or maximum tension) σ_1; (2) shear failure—at larger confining pressures the two ends of the specimen slide along a

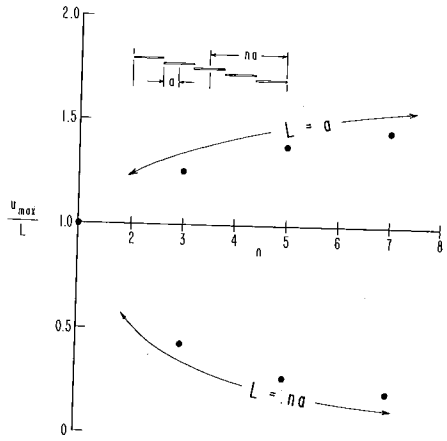

Fig. 10. Effect of number of fault segments on estimated stress change on the crack surface. Calculated maximum displacement $u_{\max}$ divided by segment half-length a (upper sequence of points) and total fault half-length na (lower sequence of points) is plotted versus the number of individual segments n.

plane or zone oriented at ≤45° to the maximum compression σ_3. We consider both styles of failure separately as mechanisms of secondary fracturing.

Extension failure is predicted when the local magnitude of maximum principal stress σ_1 equals the tensile strength. Because tensile strengths of rocks are small in magnitude, we approximate the boundary of the failure zone by the contour $\sigma_1 = 0$ (Figure 11). For left-stepping echelon cracks the area under tension is small and lies outside the cracks (Figure 11*a*). The stress orientation is such that extension fractures forming near the crack tips would propagate away from each other. For right-stepping cracks, under the same applied stresses, a much larger area of tension bridges the cracks (Figure 11*b*). Extension fractures forming near the crack tips would propagate into the region between the cracks.

The conditions for shear failure depend on both principal stresses σ_1 and σ_3 (or, equivalently, on the differential stress and confining pressure). A linear (Coulomb) relation between principal stresses at failure takes the form [*Jaeger and Cook*, 1969]

$$\sigma_1 = c_o + \sigma_3 \tan^2 (45° + \phi/2) \tag{6}$$

where c_o is the cohesion and ϕ is the internal friction angle. Rewriting (6) to conform with the tension-positive sign convention and defining $\tau = \frac{1}{2}(\sigma_1 - \sigma_3)$ and $\bar{\sigma} = \frac{1}{2}(\sigma_1 + \sigma_3)$, we find that a failure condition can be written as

$$F = a\tau + b\bar{\sigma} \tag{7}$$

where

$$a = \frac{1}{c_o}[1 + \tan^2 (45° + \phi/2)]$$

$$b = \frac{1}{c_o}[\tan^2 (45° + \phi/2) - 1]$$

Representative values of c_o and ϕ for granitic rocks are c_o = 2.3 kbar and $\phi = 33°$ [*Jaeger and Cook*, 1969], so that $a = 1.91$ and $b = -1.04$ (kbar). The material is predicted to fail on planes oriented by $45° - \phi/2$ (~30°) to the direction of maximum compression when $F = 1$ and not to fail when $F < 1$.